Letter

Nonperturbative test of nucleation calculations for strong phase transitions

Oliver Gould[*]
School of Physics and Astronomy, University of Nottingham, Nottingham NG7 2RD, United Kingdom

Anna Kormu[†] and David J. Weir[‡]
Department of Physics and Helsinki Institute of Physics, PL 64, FI-00014 University of Helsinki, Finland

(Received 7 May 2024; accepted 9 January 2025; published 31 March 2025)

Nucleation rate computations are of broad importance in particle physics and cosmology. Perturbative calculations are often used to compute the nucleation rate Γ, but these are incomplete. We perform nonperturbative lattice simulations of nucleation in a scalar field theory with a tree-level barrier, computing a final result extrapolated to the thermodynamic and continuum limits. Although the system in question should be well described by a complete one-loop perturbative calculation, we find only qualitative agreement with the full perturbative result, with a 20% discrepancy in $|\log\Gamma|$. Our result motivates further testing of the current nucleation paradigm.

DOI: 10.1103/PhysRevD.111.L051901

Introduction. First-order phase transitions in the early Universe have been of sustained interest. A primordial phase transition could help to explain the matter-antimatter asymmetry of the Universe [1–3]. The phase transition itself, as well as any resulting nonequilibrium physics of the primordial plasma, would produce a stochastic gravitational wave background that could potentially be detected [4].

Hints of a gravitational wave background have been seen by the various Pulsar Timing Array (PTA) collaborations [5–8]. Such a gravitational wave background is expected to be due to supermassive black holes [9], but it is not possible to rule out other new physics such as a phase transition [10]. Future missions such as LISA will be well placed to look for gravitational waves from electroweak-scale phase transitions [11,12], but the theoretical uncertainties in the predicted gravitational wave power spectrum will need to be constrained.

Thanks to large-scale simulations [13,14], considerable progress has been made in modeling the resulting gravitational wave power spectrum [15,16]. At the same time, the accuracy of the quantities which parametrize the power spectrum—including the nucleation rate—have faced growing scrutiny [17–22].

Experimental tests of nucleation theory in condensed matter systems show a mixed picture. For the AB transition in superfluid ^{3}He, there is a longstanding and puzzling discrepancy [23–25], whereas good agreement was found for nucleation in a ferromagnetic superfluid [26]. Recently, there have been proposals to test bubble nucleation in ultracold atomic gases [27–29].

There is a need for reliable predictions with controlled systematic uncertainties so that we can test particle physics models against gravitational wave observations, as well as for comparison with analog experiments. We focus on calibrating the accuracy of nucleation rate calculations in relativistic finite-temperature field theory, comparing perturbative semiclassical methods against direct nonperturbative numerical simulation.

At some critical temperature T_c, the effective potential energy develops two or more degenerate minima as a function of some order parameter, but the system remains in the higher-energy metastable phase even after it is energetically less favorable, as the temperature continues to fall. Eventually this will lead into bubble nucleation, where bubbles of the stable phase form.

In field theory at zero temperature, a metastable vacuum state can decay via quantum tunneling [30]. A complete one-loop calculation of the rate of this process was first carried out by Coleman and Callan [31,32], using a saddle-point approximation of the path integral. This result has since been rederived from a number of perspectives and formalisms [33–35].

At high temperature, bubbles can nucleate classically. Within classical field theory, a complete one-loop calculation for this process was first carried out by Langer [36,37], extending the tree-level theory of Cahn and Hilliard [38].

[*]Contact author: oliver.gould@nottingham.ac.uk
[†]Contact author: anna.kormu@helsinki.fi
[‡]Contact author: david.weir@helsinki.fi

Published by the American Physical Society under the terms of the Creative Commons Attribution 4.0 International license. Further distribution of this work must maintain attribution to the author(s) and the published article's title, journal citation, and DOI. Funded by SCOAP[3].

However, the analogous calculation within quantum field theory is much less clear. Early papers by Linde [39] and Affleck [40] gave slightly different expressions in the high-temperature regime. Neither agrees with the classical result of Langer.

The above methods all depend on a semiclassical picture of the bubble and its fluctuations. A fully numerical lattice calculation of the bubble nucleation rate was introduced in Ref. [41]. At the time, the focus was on the physics of the minimal Standard Model, where a first-order phase transition would have arisen from radiative corrections to the quartic Higgs potential. In Ref. [42], a toy model with similar features was studied. Recently, a more complete study of nucleation in the minimal Standard Model was carried out [43], motivated by the idea that any sufficiently heavy new particles could be integrated out [18].

Another approach has been to study thermal nucleation directly as a real-time process [44–50]. This involves evolving the lattice in time, waiting until a growing bubble appears, and recording the time taken for the bubble to appear. Since the nucleation rate can vary over many orders of magnitude, this approach is only viable over a narrow temperature range.

We consider what we call the real scalar theory [51], with the Lagrangian

$$\mathcal{L} = -\frac{1}{2}\partial_\mu\varphi\partial^\mu\varphi - V(\varphi) - J_1\varphi - J_2\varphi^2, \tag{1}$$

$$V(\varphi) = \sigma\varphi + \frac{1}{2}m^2\varphi^2 + \frac{1}{3!}g\varphi^3 + \frac{1}{4!}\lambda\varphi^4, \tag{2}$$

where σ, m^2, g, and λ are the model parameters; J_1 and J_2 represent operators of other fields; and we have used mostly plus signature. Such a scalar field may couple to the Standard Model through Higgs portal interactions (with $J_1 = \kappa_1 H^\dagger H$ and $J_2 = \kappa_2 H^\dagger H/2$), or serve as a toy model in itself to test key ideas.

Compared with radiatively induced transitions, the presence of the tree-level barrier in Eq. (2) is expected to allow for stronger transitions [52]. The perturbative expansion is also simpler [53,54], allowing us to focus on bubble nucleation without extraneous details.

We focus on the dynamics of a single bubble and its real-time evolution from the metastable phase to the stable phase. The bubbles arise as long-wavelength thermal fluctuations of the scalar field. These fluctuations are highly occupied in a thermal bath, and so their effective evolution is classical [55–57]. The effects of short-wavelength fluctuations appear both through screening of the effective parameters, and as noise and damping in the evolution equations [57,58].

Thermal fluctuations significantly modify the scalar effective potential for temperatures $T^2 \sim m^2/\lambda$ and above. At such temperatures, modes with energies of order $m \sim \sqrt{\lambda}T$ satisfy the following Langevin equation:

$$\partial_t\phi(t,\mathbf{x}) = \pi(t,\mathbf{x}), \tag{3}$$

$$\partial_t\pi(t,\mathbf{x}) = -\frac{\delta H_{\rm eff}}{\delta\phi} - \gamma\pi(t,\mathbf{x}) + \xi(t,\mathbf{x}), \tag{4}$$

where (after absorbing factors of T) ϕ is the effective field, π is its canonical momentum, γ is a damping parameter, and ξ is a local Gaussian noise term, satisfying

$$\langle\xi(t,\mathbf{x})\xi(t',\mathbf{x}')\rangle = 2\gamma\delta(t-t')\delta^{(3)}(\mathbf{x}-\mathbf{x}'). \tag{5}$$

The effective Hamiltonian, $H_{\rm eff}$, is constructed to match the long-wavelength equal-time correlation functions of the full quantum theory [59,60]. This matching reduces the long-wavelength equilibrium thermodynamics of a four-dimensional (4D) quantum field theory to that of a 3D classical statistical field theory, and hence is known as high-temperature dimensional reduction (see Sec. I in the Supplemental Material [61] for details). Importantly, for a scalar field theory, an appropriate choice of γ also leads to the matching of the unequal time correlation functions [55–57].

Saddle-point approximation. Perturbative calculations of the bubble nucleation rate are based on saddle-point approximations to the probability current between phases. To arrive at this from Eqs. (3) and (4), one introduces the probability density $P(\phi,\pi)$, which satisfies a Fokker-Planck equation [37,69]. If the metastable state is sufficiently long lived, the calculation can be set up as a static problem: one imposes boundary conditions that the metastable phase is populated thermally—$P(\phi,\pi) \propto e^{-H_{\rm eff}[\phi,\pi]}$—and the stable phase is unpopulated. There is then a constant, small flux of probability over the barrier between phases, which does not appreciably deplete the metastable state or appreciably populate the stable state [70].

For field theories, the computation of this probability current was described by Langer [36,37]. The relationship of Langer's formalism to high-temperature quantum field theories has been studied in Refs. [71,72], and generalized to higher orders in Ref. [73]. A crucial result is that the nucleation rate factorizes

$$\Gamma = A_{\rm dyn} \times A_{\rm stat}, \tag{6}$$

where $A_{\rm dyn}$ is the *dynamical* factor and $A_{\rm stat}$ is the *statistical* factor. The latter is a purely time-independent quantity, equal to the vacuum nucleation rate in $2+1$ dimensions. At leading (one-loop) order, $2\pi A_{\rm dyn}$ is equal to the initial growth rate of the critical bubble.

The statistical part takes the form of a semiclassical path integral. Its computation requires first solving for a radially symmetric saddle point of the 3D tree-level action defined in Sec. I of the Supplemental Material [61],

$$\frac{{\rm d}^2\phi}{{\rm d}r^2} + \frac{2}{r}\frac{{\rm d}\phi}{{\rm d}r} = \frac{{\rm d}V_3(\phi)}{{\rm d}\phi}. \tag{7}$$

The relevant solution, the critical bubble, has spherical symmetry. This reduces the problem to solving a one-dimensional boundary value problem, which can be solved using the shooting method [31].

With the critical bubble ϕ_b in hand, as well as the position of the metastable phase ϕ_0, the statistical part of the nucleation rate is proportional to the relative Boltzmann-weighted phase-space volume of these two stationary points,

$$A_{\text{stat}} = \sqrt{\left|\frac{\det(S''[\phi_0]/2\pi)}{\det'(S''[\phi_b]/2\pi)}\right|}\left(\frac{\Delta S[\phi_b]}{2\pi}\right)^{3/2} e^{-\Delta S[\phi_b]}, \quad (8)$$

where S'' denotes the second functional derivative of the action, the prime on det′ denotes that zero modes are not to be included, and $\Delta S[\phi_b] \equiv S[\phi_b] - S[\phi_0]$. The computation of the functional determinants can be carried out using the Gelfand-Yaglom theorem [74,75].

For the dynamical factor, one finds that

$$A_{\text{dyn}} = \frac{1}{2\pi}\left(\sqrt{|\lambda_-| + \frac{\gamma^2}{4}} - \frac{\gamma}{2}\right), \quad (9)$$

where λ_- is the single negative eigenvalue of $S''[\phi_b]$ and γ is the damping rate of Eq. (4).

For the present theory, the computation of both A_{stat} and A_{dyn} can be carried out using the numerical package BubbleDet [76], or the numerical fits from Ref. [77]. This yields our full one-loop rate, $\Gamma_{\text{one-loop}}$.

However, for applications of nucleation theory, especially for more complicated models, neither the functional determinant nor the dynamical prefactor are typically computed. In Sec. II in the Supplemental Material [61], we show two common lower-order approximations: in the first, $\Gamma_{\text{tree-level}}$, the functional determinant and dynamical prefactor are estimated as T^4, and in the second, Γ_{LPA}, a local potential approximation is made for the functional determinant, together with a prescription for dropping unwanted imaginary parts.

Lattice simulations. Our nonperturbative calculation of the nucleation rate closely follows the approach introduced in Refs. [41,42].

The lattice discretization of the action takes the form

$$S_{\text{lat}} = \sum_x a^3\left[-\frac{1}{2}Z_\phi\phi_x(\nabla^2_{\text{lat}}\phi)_x + \sigma_{\text{lat}}\phi_x + \frac{1}{2}Z_\phi Z_m m^2_{\text{lat}}\phi_x^2 + \frac{1}{4!}Z_\phi^2\lambda_{\text{lat}}\phi_x^4\right], \quad (10)$$

where the sum over x extends over the 3D lattice sites. We have removed the cubic term by a constant shift in the field. One can derive exact lattice-continuum relations for this model within lattice perturbation theory [78], and improvements up to $O(a^2)$ [42,79,80]. See Sec. III in the Supplemental Material [61] for more information about our lattice action and [81] for the simulation code.

There are two stages: lattice Monte Carlo simulations which generate configurations, some of which lie close to the separatrix (sometimes known as the "transition surface" [37,71]) of field configurations between the two phases. Selected near-separatrix configurations are then evolved numerically in a thermal bath to determine whether they tunnel or not.

Critical bubble probability: The separatrix configurations are suppressed by $\sim e^{-65}$ at the temperature we simulate. Our Monte Carlo simulations therefore use the multicanonical method [82,83] to overcome this suppression and generate a sufficient number of near-critical bubble configurations (see Ref. [51] for its application to the current model). The order parameter θ_{op} is measured, yielding a histogram that (below T_c) will resemble Fig. 1. If the choice of order parameter, system volume, and geometry admit, then there will be a local minimum between the metastable and stable phase peaks that we identify with the separatrix, at $\theta_{\text{op}} = \theta_c$. This corresponds to critical bubble configurations. Configurations sufficiently near the separatrix $\theta_{\text{op}} \in [\theta_c - \frac{\epsilon}{2}, \theta_c + \frac{\epsilon}{2}]$ are used as the initial conditions for evolution of the lattice versions of the stochastic evolution equations (3) and (4), along with momenta drawn from a Gaussian distribution. The final result is independent of the exact choice of ϵ, but it should be sufficiently small that the sampled configurations correspond to near-critical bubbles.

From the selected near-separatrix field configurations, we can determine the probabilities $P(\theta_{\text{op}})$ for the critical bubble and metastable phases, and we normalize the probability of being in the critical configuration to that of the metastable phase,

$$P_c^{\text{normalized}} = \frac{P(|\theta_{\text{op}} - \theta_c| < \epsilon/2)}{\epsilon P(\theta_{\text{op}} < \theta_c)}. \quad (11)$$

Effective tunneling fraction: Following Ref. [42], the dynamical information can be separated into two parts:

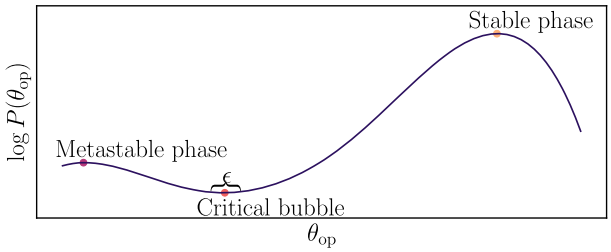


FIG. 1. Probability distribution $P(\theta_{\text{op}})$ of the order parameter at some temperature below T_c. The metastable and stable phases are separated by an exponentially suppressed area, the mixed critical bubble. The separatrix configurations are drawn from the narrow range ϵ around the critical bubble.

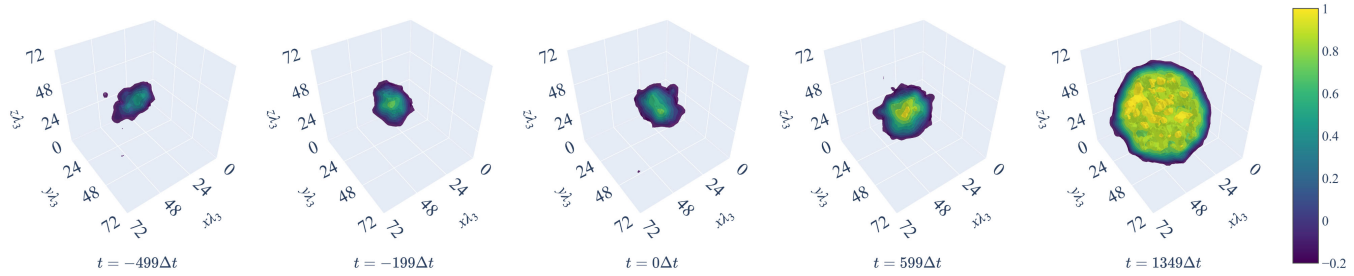


FIG. 2. Snapshots of a nucleating bubble with lattice size $L\lambda_3 = 72$ and spacing $a\lambda_3 = 1.5$. We remove ultraviolet fluctuations by performing eight steps of nearest-neighbor averaging. Here, $t = 0\Delta t$ corresponds to the initial separatrix configuration, and the negative time direction describes the backward time evolution. Note that the snapshots are not evenly spaced in time.

the flux—the rate of change of the order parameter as it crosses the separatrix, and **d**—the ratio of tunneled configurations determined by real time trajectories. To determine whether a configuration tunnels or not, we directly evolve the stochastic Hamiltonian equations, (3) and (4), both forwards and backwards in time, with the initial momenta reversed for the backwards evolution (see Fig. 2). We use a time step $\Delta t\lambda_3 = 0.01$ much smaller than the lattice spacing.

If a given trajectory begins and ends in different phases (either metastable → stable or vice versa), we set $\delta_{\text{tunnel}} = 1$; otherwise, $\delta_{\text{tunnel}} = 0$. The ratio of tunneled trajectories is an observable defined for each trajectory as

$$\mathbf{d} = \frac{\delta_{\text{tunnel}}}{N_{\text{crossings}}}, \tag{12}$$

where $N_{\text{crossings}}$ is the number of times the given trajectory crosses θ_c. Lastly, we must add a factor of $\frac{1}{2}$ to account for metastable → stable trajectories only, to avoid double-counting the tunneled trajectories.

The full nucleation rate on the lattice is a combination of the above three elements:

$$\Gamma\mathcal{V} = P_c^{\text{normalized}}\left\langle \frac{1}{2}\text{flux} \times \mathbf{d} \right\rangle, \tag{13}$$

where $\mathcal{V}$ is the lattice volume.

For field-theory systems with many degrees of freedom, the flux is dominated by uncorrelated short-time fluctuations, whereas the global behavior of the trajectories depends on longer-time correlations. These are therefore assumed to be uncorrelated, and we approximate the rate by

$$\Gamma\mathcal{V} \approx P_c^{\text{normalized}}\frac{1}{2}\langle\text{flux}\rangle\langle\mathbf{d}\rangle. \tag{14}$$

These formulas are order-parameter independent, but the choice of order parameter affects the viability of this method. At larger volumes, the contribution of bulk fluctuations about the metastable minimum will in general grow relative to the critical bubble. The physical volume occupied by the critical bubble is fixed, so that eventually bulk fluctuations dominate.

The flux through the critical separatrix surface is order-parameter dependent. It can be solved analytically due to the Gaussianity of the momentum field [42]

$$\langle\text{flux}\rangle = \left\langle \left|\frac{\Delta\theta_{\text{op}}}{\Delta t}\right|_{\theta_c} \right\rangle = \sqrt{\frac{8}{\pi\mathcal{V}}(\theta_c + A^2)}, \tag{15}$$

where our order parameter $\theta_{\text{op}} = \overline{\phi^2} - 2A\bar{\phi}$, and A is a constant, which we choose to be the peak of the histogram of ϕ in the metastable phase. We have used an overbar to mean volume averaging and angle brackets for statistical averaging. We also considered $\theta'_{\text{op}} = \bar{\phi}$ [with corresponding flux $\sqrt{2/(\pi\mathcal{V})}$] but found that bulk fluctuations affected our ability to go to large volumes with this choice.

Results: In Fig. 3, we show how the obtained nucleation rate varies with lattice spacing and volume. The dependence on both is rather mild, allowing us to take controlled continuum extrapolations.

Given our use of an $O(a^2)$ improved lattice discretization, the leading dependence on lattice spacing arises at $O(a^3)$. For a fixed volume of $L\lambda_3 = 42$, we vary the lattice spacing and perform a least-squares fit $f(a) = b + ca^3$ to the logarithm of the rate. The best-fit line, with $\chi^2/\text{d.o.f.} = 0.79$, excluding $\lambda_3 a = 3.5$, is plotted in the figure. Jackknife-resampling this fit yields $\log(\Gamma/\lambda_3^4) = -73.24(11)$. Our largest lattice spacing $a\lambda_3 = 3.5$ is approximately the inverse screening mass of the system—a one-loop estimate of the screening mass yields $m_s^{\text{PT}}/\lambda_3 = 0.294(1)$ [51]—at which point the cubic form is expected to break down. Motivated by this, we fit $f(a) = b + ca^3 + da^4$ to all data points, giving $\chi^2/\text{d.o.f.} = 1.76$. We find agreement on the fit parameters between the two approaches. From the figure, we deduce that lattice artifacts are comparable to statistical uncertainties already with $\lambda_3 a = 1.5$.

For reference, we also show the nucleation rate computed using the linear-order parameter $\theta_{\text{op}} = \phi_{\text{lin}}$ for one lattice spacing. We find agreement within error with our final results; however, our quadratic-order parameter shows substantially reduced errors, which we attribute to the relative suppression of the metastable phase bulk fluctuations.

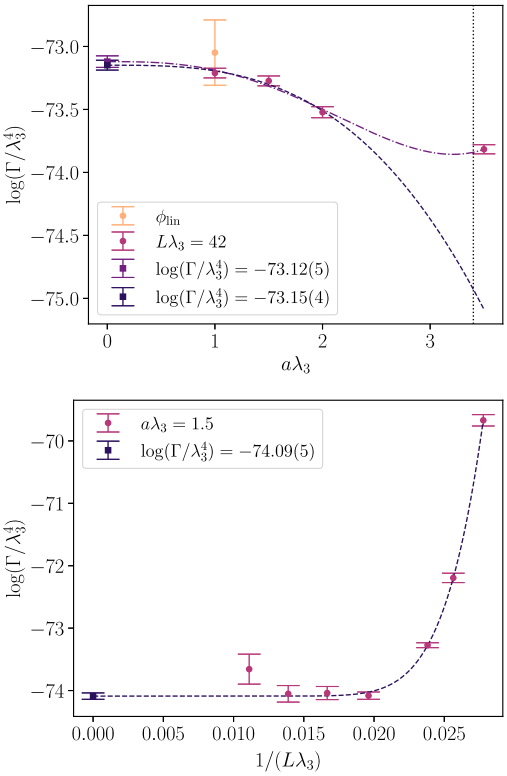


FIG. 3. The zero-lattice-spacing (top) and infinite-volume (bottom) extrapolations, together with cubic, cubic plus quartic, and exponential fits. The vertical line in the top plot marks a perturbative estimate of the correlation length.

We then show the dependence on volume at constant lattice spacing $\lambda_3 a = 1.5$. Away from the second-order phase transition, this 3D Euclidean model has no massless modes, so long-range correlations die off exponentially with distance. Motivated by this, we fit the logarithm of the rate to an exponential $f(L) = b + c\exp(-m_s L)$, finding $m_s/\lambda_3 = 0.283(12)$, consistent with the perturbative screening mass. We show the best-fit line in the figure, with $\chi^2/\text{d.o.f.} = 1.54$. Jackknife-resampling this fit yields $\log(\Gamma/\lambda_3^4) = -74.09(5)$ for the infinite-volume extrapolation. Note that fitting $f(L) = b + c/L^n$ with $n \in \{1, 2, 3\}$ to our finite-volume data yields much poorer fits, with $\chi^2/\text{d.o.f.} \sim 10^2$.

Even with our improved choice of order parameter, we are limited in the largest volume we can reach for a number of reasons. For sufficiently large volumes, critical bubble configurations are again buried under the bulk fluctuations of the metastable phase. Nevertheless, we see that the bubble is well resolved for the volumes we simulate in two ways: both geometrically determining which interface geometry (bubble, cylinder, or slab) is favored in the thin-wall approximation [41], and also visual inspection of configurations show a well-resolved spherical bubble configuration; see Fig. 2.

Discussion. The main result of this work is the logarithm of the nucleation rate, reliably computed to high precision for a real scalar quantum field theory at high temperature. Statistical uncertainties are much smaller than discrepancies with other methods, as seen in Fig. 4. Systematic uncertainties related to the continuum extrapolation are also well under control, as evidenced by Fig. 3. This has been made possible by the use of efficient multicanonical algorithms [41,42,82,83], and exact and $O(a^2)$ improved lattice-continuum relations [42,78–80].

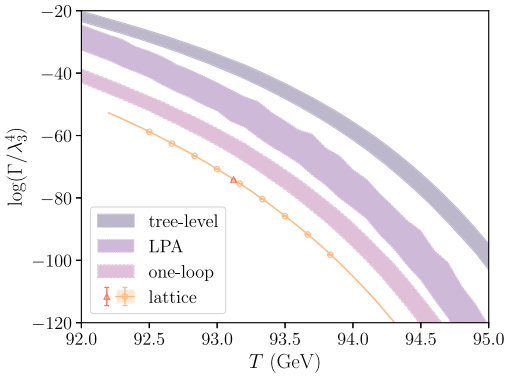


FIG. 4. The nucleation rate as a function of temperature. Uncertainty bands for the tree-level and one-loop perturbative results are based on varying the renormalization scale over $\mu_3/\lambda_3 \in \{0.5, 1, 2\}$. The uncertainty estimate on the LPA reflects different choices for removing imaginary parts of the potential. The lattice points are continuum-extrapolated: the red triangle highlights the temperature actually simulated, while the orange circles have utilized reweighting. The orange continuous line is the reweighted result for $a\lambda_3 = 1.5$, $L\lambda_3 = 60$. The results in this figure are tabulated in Ref. [84].

The benchmark parameter point that we simulated was chosen with the hope of testing perturbation theory in a regime where it is expected to work well.[1] The loop expansion converges rapidly for the field condensate (adopting units where $\lambda_3 = 1$) [51]

$$\Delta\langle\phi\rangle_c^{\rm lat} = 1.341(2), \qquad \Delta\langle\phi\rangle_c^{\rm pt} = 1.2 + 0.1378 + \cdots. \quad (16)$$

We have displayed the first two terms of the loop expansion within the 3D EFT. The tree-level prediction agrees with the lattice to 10%, and at one-loop to 0.2%. The two- and three-loop terms are smaller still. In Sec. III C, we have also found that the lattice and one-loop estimates of the screening mass agree within statistical uncertainties.

Yet for the nucleation rate at the temperature simulated, and at the same physical parameter point, we have

$$|\log\Gamma|^{\rm lat} = 74.09(5), \qquad |\log\Gamma|^{\rm pt} = 38.0 + 25.3 + \cdots. \quad (17)$$

[1]For our chosen xSM parameter point in 4D, at one loop we find $T_c \approx 98.5$ GeV, $\Delta\langle\varphi\rangle_c/T_c \approx 1.67$, and the percolation temperature is $T_* \approx 94.8$ GeV [11].

One might expect that this lack of convergence could be explained by the growth of the loop expansion parameter as the system supercools, which becomes almost twice as large at the temperature we have simulated than at the critical temperature. However, even at twice larger couplings, the discontinuity in the field condensate agrees to within 20% at tree level and 2% at one loop [51]. Note that the discrepancy in the rate cannot be explained by an offset in temperature, as both lattice and perturbation theory use the same EFT parameters, and in this model the critical temperature is fixed by the Z_2 symmetry between phases, and hence, it is exact already at tree level within the 3D EFT [51].

However, what if the discrepancy between the one-loop and lattice results cannot be explained simply by the next loop order? While the critical bubble is a saddle point of the path integral, there may be other relevant saddle points [85,86]. Further, for such weakly damped systems, it has been argued that the saddle-point approximation itself breaks down for the dynamical part of the nucleation rate [73,87]. Alternatively, a number of suggestions have been put forward to resolve the longstanding discrepancy between theory and experiment for the nucleation rate between the A and B phases of superfluid ^{3}He, including resonant tunneling and tunneling via intermediate solitonic configurations [88,89].

As far as we are aware, there has never been a calculation of the thermal nucleation rate of any quantum field theory beyond one-loop order. To really test whether perturbation theory provides a reliable guide to bubble nucleation, a complete two-loop calculation at our benchmark point provides a clear target for future work. Further, nonperturbative results over a range of couplings could test convergence.

For phenomenological studies of cosmological phase transitions, and their gravitational wave signals, our results demonstrate that the widely used tree-level and local potential approximations give relatively poor accuracy for the logarithm of the bubble nucleation rate. The full one-loop approximation fares significantly better. This calculation can be carried out in simple models using existing numerical tools [76], but it is still out of reach for, e.g., scalar extensions of the Standard Model.

While our lattice simulations give reliable and precise predictions for the nucleation rate, their calculation is slow. To use such lattice simulations for phenomenological studies of cosmological phase transitions, faster sampling of the relevant bubble configurations is needed. We have identified one direction of progress, through the development of order parameters optimized to enhance the sampling of tunneling configurations. Our quadratic-order parameter $\theta_{\rm op} = \bar{\phi}^2 - 2A\bar{\phi}$ was crucial for efficiently simulating the larger volumes.

Acknowledgments. The authors would like to thank Kari Rummukainen for his insights and advice at a number of points throughout this study. O. G. was supported by the Research Funds of the University of Helsinki, the UK Science and Technology Facilities Council (STFC) Consolidated Grant No. ST/T000732/1, a Research Leadership Award from the Leverhulme Trust, and a Royal Society Dorothy Hodgkin Fellowship. A. K. was supported by Research Council of Finland Grant No. 328958 and a travel grant from the Jenny and Antti Wihuri Foundation. D. J. W. was supported by Research Council of Finland Grants No. 324882, No. 328958, No. 349865, and No. 353131. The authors also wish to acknowledge the CSC-IT Center for Science, Finland, for computational resources.

Data availability. The data that support the findings of this article are openly available [84].

[1] V. A. Kuzmin, V. A. Rubakov, and M. E. Shaposhnikov, On the anomalous electroweak baryon number nonconservation in the early universe, Phys. Lett. **155B**, 36 (1985).
[2] J. M. Cline, A. Friedlander, D.-M. He, K. Kainulainen, B. Laurent, and D. Tucker-Smith, Baryogenesis and gravity waves from a UV-completed electroweak phase transition, Phys. Rev. D **103**, 123529 (2021).
[3] J. Ellis, M. Lewicki, M. Merchand, J. M. No, and M. Zych, The scalar singlet extension of the standard model: Gravitational waves versus baryogenesis, J. High Energy Phys. 01 (2023) 093.
[4] M. B. Hindmarsh, M. Lüben, J. Lumma, and M. Pauly, Phase transitions in the early universe, SciPost Phys. Lect. Notes **24**, 1 (2021).
[5] G. Agazie *et al.* (NANOGrav Collaboration), The NANOGrav 15 yr data set: Evidence for a gravitational-wave background, Astrophys. J. Lett. **951**, L8 (2023).
[6] J. Antoniadis *et al.* (EPTA, InPTA Collaborations), The second data release from the European Pulsar Timing Array—III. Search for gravitational wave signals, Astron. Astrophys. **678**, A50 (2023).
[7] H. Xu *et al.*, Searching for the nano-hertz stochastic gravitational wave background with the Chinese Pulsar Timing Array Data Release I, Res. Astron. Astrophys. **23**, 075024 (2023).
[8] D. J. Reardon *et al.*, Search for an isotropic gravitational-wave background with the Parkes Pulsar Timing Array, Astrophys. J. Lett. **951**, L6 (2023).

[9] G. Agazie *et al.* (NANOGrav Collaboration), The NANOGrav 15 yr data set: Constraints on supermassive black hole binaries from the gravitational-wave background, Astrophys. J. Lett. **952**, L37 (2023).
[10] A. Afzal *et al.* (NANOGrav Collaboration), The NANOGrav 15 yr data set: Search for signals from new physics, Astrophys. J. Lett. **951**, L11 (2023).
[11] C. Caprini *et al.*, Detecting gravitational waves from cosmological phase transitions with LISA: An update, J. Cosmol. Astropart. Phys. 03 (2020) 024.
[12] P. Auclair *et al.* (LISA Cosmology Working Group), Cosmology with the laser interferometer space antenna, Living Rev. Relativity **26**, 5 (2023).
[13] M. Hindmarsh, S. J. Huber, K. Rummukainen, and D. J. Weir, Shape of the acoustic gravitational wave power spectrum from a first order phase transition, Phys. Rev. D **96**, 103520 (2017); **101**, 089902(E) (2020).
[14] R. Jinno, T. Konstandin, H. Rubira, and I. Stomberg, Higgsless simulations of cosmological phase transitions and gravitational waves, J. Cosmol. Astropart. Phys. 02 (2023) 011.
[15] T. Konstandin, Gravitational radiation from a bulk flow model, J. Cosmol. Astropart. Phys. 03 (2018) 047.
[16] M. Hindmarsh and M. Hijazi, Gravitational waves from first order cosmological phase transitions in the Sound Shell Model, J. Cosmol. Astropart. Phys. 12 (2019) 062.
[17] K. Kainulainen, V. Keus, L. Niemi, K. Rummukainen, T. V. I. Tenkanen, and V. Vaskonen, On the validity of perturbative studies of the electroweak phase transition in the Two Higgs Doublet model, J. High Energy Phys. 06 (2019) 075.
[18] O. Gould, J. Kozaczuk, L. Niemi, M. J. Ramsey-Musolf, T. V. I. Tenkanen, and D. J. Weir, Nonperturbative analysis of the gravitational waves from a first-order electroweak phase transition, Phys. Rev. D **100**, 115024 (2019).
[19] A. Ekstedt and J. Löfgren, A critical look at the electroweak phase transition, J. High Energy Phys. 12 (2020) 136.
[20] D. Croon, O. Gould, P. Schicho, T. V. I. Tenkanen, and G. White, Theoretical uncertainties for cosmological first-order phase transitions, J. High Energy Phys. 04 (2021) 055.
[21] O. Gould and T. V. I. Tenkanen, On the perturbative expansion at high temperature and implications for cosmological phase transitions, J. High Energy Phys. 06 (2021) 069.
[22] A. Ekstedt, Convergence of the nucleation rate for first-order phase transitions, Phys. Rev. D **106**, 095026 (2022).
[23] P. Schiffer, D. Osheroff, and A. Leggett, Nucleation of the AB transition in superfluid ^{3}He: Experimental and theoretical considerations, in *Progress in Low Temperature Physics* (Elsevier, New York, 1995), Vol. 14, pp. 159–211, 10.1016/S0079-6417(06)80017-X.
[24] Y. Tian *et al.*, Supercooling of the A phase of ^{3}He, Nat. Commun. **14**, 148 (2023).
[25] M. Hindmarsh *et al.*, A-B transition in superfluid ^{3}He and cosmological phase transitions, J. Low Temp. Phys. **215**, 495 (2024).
[26] A. Zenesini, A. Berti, R. Cominotti, C. Rogora, I. G. Moss, T. P. Billam, I. Carusotto, G. Lamporesi, A. Recati, and G. Ferrari, Observation of false vacuum decay via bubble formation in ferromagnetic superfluids, Nat. Phys. **20**, 558 (2024).
[27] O. Fialko, B. Opanchuk, A. I. Sidorov, P. D. Drummond, and J. Brand, The universe on a table top: Engineering quantum decay of a relativistic scalar field from a metastable vacuum, J. Phys. B **50**, 024003 (2017).
[28] T. P. Billam, R. Gregory, F. Michel, and I. G. Moss, Simulating seeded vacuum decay in a cold atom system, Phys. Rev. D **100**, 065016 (2019).
[29] A. C. Jenkins, J. Braden, H. V. Peiris, A. Pontzen, M. C. Johnson, and S. Weinfurtner, Analog vacuum decay from vacuum initial conditions, Phys. Rev. D **109**, 023506 (2024).
[30] I. Y. Kobzarev, L. B. Okun, and M. B. Voloshin, Bubbles in metastable vacuum, Yad. Fiz. **20**, 1229 (1974).
[31] S. R. Coleman, The fate of the false vacuum. 1. Semiclassical theory, Phys. Rev. D **15**, 2929 (1977); **16**, 1248(E) (1977).
[32] C. G. Callan, Jr. and S. R. Coleman, The fate of the false vacuum. 2. First quantum corrections, Phys. Rev. D **16**, 1762 (1977).
[33] A. D. Plascencia and C. Tamarit, Convexity, gauge-dependence and tunneling rates, J. High Energy Phys. 10 (2016) 099.
[34] A. Andreassen, D. Farhi, W. Frost, and M. D. Schwartz, Direct approach to quantum tunneling, Phys. Rev. Lett. **117**, 231601 (2016).
[35] W.-Y. Ai, B. Garbrecht, and C. Tamarit, Functional methods for false vacuum decay in real time, J. High Energy Phys. 12 (2019) 095.
[36] J. S. Langer, Theory of the condensation point, Ann. Phys. (N.Y.) **41**, 108 (1967).
[37] J. S. Langer, Statistical theory of the decay of metastable states, Ann. Phys. (N.Y.) **54**, 258 (1969).
[38] J. W. Cahn and J. E. Hilliard, Free energy of a nonuniform system. III. Nucleation in a two-component incompressible fluid, J. Chem. Phys. **31**, 688 (1959).
[39] A. D. Linde, Fate of the false vacuum at finite temperature: Theory and applications, Phys. Lett. **100B**, 37 (1981).
[40] I. Affleck, Quantum statistical metastability, Phys. Rev. Lett. **46**, 388 (1981).
[41] G. D. Moore and K. Rummukainen, Electroweak bubble nucleation, nonperturbatively, Phys. Rev. D **63**, 045002 (2001).
[42] G. D. Moore, K. Rummukainen, and A. Tranberg, Nonperturbative computation of the bubble nucleation rate in the cubic anisotropy model, J. High Energy Phys. 04 (2001) 017.
[43] O. Gould, S. Güyer, and K. Rummukainen, First-order electroweak phase transitions: A nonperturbative update, Phys. Rev. D **106**, 114507 (2022).
[44] D. Y. Grigoriev and V. A. Rubakov, Soliton pair creation at finite temperatures. Numerical study in $(1+1)$-dimensions, Nucl. Phys. **B299**, 67 (1988).
[45] O. T. Valls and G. F. Mazenko, Nucleation in a time-dependent Ginzburg-Landau model: A numerical study, Phys. Rev. B **42**, 6614 (1990).
[46] M. G. Alford, H. Feldman, and M. Gleiser, Thermal activation of metastable decay: Testing nucleation theory, Phys. Rev. D **47**, R2168 (1993).
[47] M. G. Alford and M. Gleiser, Metastability in two-dimensions and the effective potential, Phys. Rev. D **48**, 2838 (1993).

[48] S. Borsanyi, A. Patkos, J. Polonyi, and Z. Szep, Fate of the classical false vacuum, Phys. Rev. D **62**, 085013 (2000).

[49] L. Batini, A. Chatrchyan, and J. Berges, Real-time dynamics of false vacuum decay, Phys. Rev. D **109**, 023502 (2024).

[50] D. Pîrvu, M. C. Johnson, and S. Sibiryakov, Bubble velocities and oscillon precursors in first order phase transitions, J. High Energy Phys. 11 (2024) 064.

[51] O. Gould, Real scalar phase transitions: A nonperturbative analysis, J. High Energy Phys. 04 (2021) 057.

[52] D. J. H. Chung, A. J. Long, and L.-T. Wang, 125 GeV Higgs boson and electroweak phase transition model classes, Phys. Rev. D **87**, 023509 (2013).

[53] A. Ekstedt, O. Gould, and J. Löfgren, Radiative first-order phase transitions to next-to-next-to-leading order, Phys. Rev. D **106**, 036012 (2022).

[54] O. Gould and T. V. I. Tenkanen, Perturbative effective field theory expansions for cosmological phase transitions, J. High Energy Phys. 01 (2024) 048.

[55] G. Aarts and J. Smit, Classical approximation for time dependent quantum field theory: Diagrammatic analysis for hot scalar fields, Nucl. Phys. **B511**, 451 (1998).

[56] D. Bodeker, Classical real time correlation functions and quantum corrections at finite temperature, Nucl. Phys. **B486**, 500 (1997).

[57] C. Greiner and B. Muller, Classical fields near thermal equilibrium, Phys. Rev. D **55**, 1026 (1997).

[58] M. Morikawa, Classical fluctuations in dissipative quantum systems, Phys. Rev. D **33**, 3607 (1986).

[59] K. Kajantie, M. Laine, K. Rummukainen, and M. E. Shaposhnikov, Generic rules for high temperature dimensional reduction and their application to the standard model, Nucl. Phys. **B458**, 90 (1996).

[60] E. Braaten and A. Nieto, Effective field theory approach to high temperature thermodynamics, Phys. Rev. D **51**, 6990 (1995).

[61] See Supplemental Material at http://link.aps.org/supplemental/10.1103/PhysRevD.111.L051901 for more details on the high-temperature effective field theory setup and lattice calculation, which includes Refs. [62–68].

[62] E. J. Weinberg and A.-q. Wu, Understanding complex perturbative effective potentials, Phys. Rev. D **36**, 2474 (1987).

[63] C. L. Wainwright, CosmoTransitions: Computing cosmological phase transition temperatures and bubble profiles with multiple fields, Comput. Phys. Commun. **183**, 2006 (2012).

[64] C. Delaunay, C. Grojean, and J. D. Wells, Dynamics of nonrenormalizable electroweak symmetry breaking, J. High Energy Phys. 04 (2008) 029.

[65] P. Athron, C. Balazs, A. Fowlie, L. Morris, G. White, and Y. Zhang, How arbitrary are perturbative calculations of the electroweak phase transition?, J. High Energy Phys. 01 (2023) 050.

[66] E. Forest and R. D. Ruth, Fourth order symplectic integration, Physica (Amsterdam) **43D**, 105 (1990).

[67] A. M. Horowitz, A generalized guided Monte Carlo algorithm, Phys. Lett. B **268**, 247 (1991).

[68] H. Yoshida, Construction of higher order symplectic integrators, Phys. Lett. A **150**, 262 (1990).

[69] A. Berera, J. Mabillard, B. W. Mintz, and R. O. Ramos, Formulating the Kramers problem in field theory, Phys. Rev. D **100**, 076005 (2019).

[70] H. A. Kramers, Brownian motion in a field of force and the diffusion model of chemical reactions, Physica **7**, 284 (1940).

[71] O. Gould and J. Hirvonen, Effective field theory approach to thermal bubble nucleation, Phys. Rev. D **104**, 096015 (2021).

[72] J. Hirvonen, Nucleation rate in a high-temperature quantum field theory with hard particles, arXiv:2403.07987.

[73] A. Ekstedt, Bubble nucleation to all orders, J. High Energy Phys. 08 (2022) 115.

[74] I. M. Gelfand and A. M. Yaglom, Integration in functional spaces and it applications in quantum physics, J. Math. Phys. (N.Y.) **1**, 48 (1960).

[75] J. Baacke and V. G. Kiselev, One loop corrections to the bubble nucleation rate at finite temperature, Phys. Rev. D **48**, 5648 (1993).

[76] A. Ekstedt, O. Gould, and J. Hirvonen, BubbleDet: A Python package to compute functional determinants for bubble nucleation, J. High Energy Phys. 12 (2023) 056.

[77] A. Ekstedt, Higher-order corrections to the bubble-nucleation rate at finite temperature, Eur. Phys. J. C **82**, 173 (2022).

[78] M. Laine, Exact relation of lattice and continuum parameters in three-dimensional $\mathrm{SU}(2) + \mathrm{Higgs}$ theories, Nucl. Phys. **B451**, 484 (1995).

[79] P. B. Arnold and G. D. Moore, Monte Carlo simulation of O(2) φ^4 field theory in three-dimensions, Phys. Rev. E **64**, 066113 (2001); **68**, 049902(E) (2003).

[80] X.-p. Sun, Monte Carlo studies of three-dimensional O(1) and O(4) φ^4 theory related to BEC phase transition temperatures, Phys. Rev. E **67**, 066702 (2003).

[81] O. Gould, A. Kormu, and D. J. Weir, Scalnuc release 2.1.0. (2025), https://archive.softwareheritage.org/browse/release/94596986a4cf3bfd61ed75e34de3fe46a66d4753/?origin_url=https://bitbucket.org/og113/scalnuc.git&snapshot=85d8b3bf7b4550676db3ca4913273cd89ea0a40f.

[82] B. A. Berg and T. Neuhaus, Multicanonical algorithms for first order phase transitions, Phys. Lett. B **267**, 249 (1991).

[83] B. A. Berg and T. Neuhaus, Multicanonical ensemble: A new approach to simulate first order phase transitions, Phys. Rev. Lett. **68**, 9 (1992).

[84] O. Gould, A. Kormu, and D. Weir, Final data for paper "a nonperturbative test of nucleation calculations for strong phase transitions", 10.5281/zenodo.10891523 (2024).

[85] A. Andreassen, D. Farhi, W. Frost, and M. D. Schwartz, Precision decay rate calculations in quantum field theory, Phys. Rev. D **95**, 085011 (2017).

[86] J. Braden, M. C. Johnson, H. V. Peiris, A. Pontzen, and S. Weinfurtner, New semiclassical picture of vacuum decay, Phys. Rev. Lett. **123**, 031601 (2019); **129**, 059901(E) (2022).

[87] P. Hanggi, P. Talkner, and M. Borkovec, Reaction-rate theory: Fifty years after Kramers, Rev. Mod. Phys. **62**, 251 (1990).

[88] D. K. Hong, Q balls in superfluid ^{3}He, J. Low Temp. Phys. **71**, 483 (1988).

[89] S. H. H. Tye and D. Wohns, Resonant tunneling in superfluid Helium-3, Phys. Rev. B **84**, 184518 (2011).